RESEARCH ARTICLE OPEN ACCESS

Structural and Dielectric Properties of Pb^{2+} Doped ZnO Nanocrystalline Thin Films

N. Nithya[a,*] and S. Rugmini Radhakrishnan[b]
[a]Department of Physics, Tamilnadu College of Engineering, Coimbatore – 641659, Tamilnadu, India.
[b]Department of Physics, Avinashilingam Institute for Home Science and Higher Education for Women, Coimbatore - 641043, Tamilnadu, India.

Abstract
Various concentration of lead (Pb^{2+}) doped ZnO nanocrystalline thin films were prepared by chemical bath deposition and dielectric constant, dielectric loss and AC conductivity properties were studied as a function of frequency at different temperatures. The XRD results revealed that prepared nanocrystalline films have wrutzite structure and the crystallite sizes of doped ZnO increased with increasing Pb^{2+} concentration. The variation of AC conductivity (σ_{ac}) as function of temperature indicates that the conduction is due to thermally activated charge carriers. The DC conductivity (σ_{dc}) value of doped ZnO at room temperature has been found to increase by more than two orders of magnitude from pure ZnO nanocrystalline thin film. The AC electrical conductivity of doped films is higher than that of pure ZnO film. The observed σ_{ac} values are found to be more than σ_{dc} values.
Key words: Nanocrystalline thin film, CBD, XRD, TEM, dielectric constant, dielectric loss, AC conductivity, DC conductivity

I. Introduction

ZnO is one of the promising II-VI semiconducting materials has been extensively developed for many applications such as transparent conducting electrodes, sensors, antireflection coatings in solar cells, liquid crystal displays, heat mirrors, surface acoustic wave devices [1-14]. In particular, cost-effective transparent conductive ZnO thin film is eminently suitable for use in transparent electrodes for flat panel display and solar cells on large area substrates and UV-emitting diodes, ultraviolet laser and in optoelectronics such as light emitting diodes, photodetectors, transparent thin-film transistors, field emitters, field effect transistors and various other devices [15-25]. It is a non-toxic, n type, direct wide band gap material (E_g = 3.3eV at 300K) with good electrical conductivity and high optical transparency in the visible and near infrared region.

As is well known, doping suitable elements in ZnO film offers an effective method to engineer their electrical and optical properties. Recently, many elements such as Al, Mg, Ga, S, Ag, Ti, Cu and Pb [26-39] have been doped or alloyed into ZnO film and good properties have been obtained. Among the various types of doped ZnO thin films Pb has many physical and chemical properties that are similar to those of Zn. Pb doping has been reported to be able to change the electrical, optical and microstructure properties of ZnO thin films. The catalytic effect of lead on the micro structural, optical properties has been extensively reported in many works [40-41]. However, no reports are available for electrical conductivity of Pb doped ZnO nanocrystals. The incorporation of Pb can change the resistive switching properties of ZnO films. Therefore, the amount of lead is one of the key factors affecting the quality of the ZnO:Pb film. It is necessary to study the effects of lead in order to develop ZnO:Pb film with high quality and good performance.

In our previous work, for example, chemical bath deposition (CBD) technique has been used to prepare ZnO:Cu^{2+} and ZnO:Mn^{2+} nanocrystalline thin films with different dopant concentrations [42-43]. In the present work we report the preparation of Pb^{2+}-doped ZnO thin films with lead compositions in the range of 0–10.0 mole % insteps of 2.5 mole % using simple and cost effective chemical bath deposition method (CBD), and the influences of Pb^{2+} concentration on the structural and electrical properties of films are discussed in detail.

II. Experimental procedure

Undoped and Pb^{2+} doped ZnO nanocrystalline films, at the Pb^{2+} percentages of 2.5, 5.0, 7.5 and 10.0 mole % were deposited using an chemical bath deposition (CBD) technique described elsewhere [42].

The deposited films were characterized for their structural properties using the appropriate techniques. The crystalline structure of the films was confirmed by X-ray diffraction (XRD) with Cu K_α radiation (PANalytical X-Pert Pro diffractometer, λ =

1.54056 Å). The accelerating voltage of 40 kV, emission current of 30 mA and the scanning speed of 2º per min were used. The crystallite size analysis was made using Scherrer method [44]. The DC electrical conductivity measurements were carried out to an accuracy of ± 1% for all the synthesized pure and doped thin film using the conventional four-probe technique. The measurements were made at various temperatures ranging from 30 - 150ºC. The resistances of the thin film samples were measured using a four probe technique. The samples were again annealed in the holder assembly at ~160ºC before making observations. The observations were made while cooling the sample. Temperature was controlled to an accuracy of ± 0.5ºC. The voltage drops (V) across the samples were measured at constant current (I). The thickness of the thin film samples were measured using a thin film thickness measuring unit model US M probe Vis. spectroscopic reflectometer. The DC conductivity (σ_{dc}) of the crystal was calculated using the relation

$$\sigma_{dc} = \frac{I}{V\, 2\, \pi\, S} \quad \text{mho m}^{-1},$$

where V is the measured voltage drop across the sample, S is the surface area covered by the electrode on the thin film sample and.

The capacitance (C) and dielectric loss factor (tanδ) measurements were carried out to an accuracy of ± 1 % with Agilant 4284A LCR meter in the various temperatures of 30 – 150 ºC and with different frequencies ranges from 100 Hz to 1 MHz by using conventional two-probe technique [45]. The samples were prepared and annealed in a way similar to that followed for the dc conductivity measurement. The observations were made while cooling the sample. Temperature was controlled to an accuracy of ± 1ºC. Air capacitance (C_{air}) was also measured. The dielectric constant (ε_r) of the crystal was calculated using the relation,

$$\varepsilon_r = \frac{C}{C_{air}}$$

The AC electrical conductivity (σ_{ac}) was calculated using the relation

$$\sigma_{ac} = \varepsilon_o\, \varepsilon_r\, \omega \tan\delta,$$

where ε_o is the permittivity of free space (8.854 x 10^{-12} F/m) and ω is the angular frequency (ω = 2πf; f = 100Hz to 1 MHz in the present study).

III. Results and discussion

3.1. Structural studies

The crystal structure and orientation of the as-deposited Pb^{2+} doped ZnO thin film samples were investigated using XRD and the results are depicted in Fig. 1(a and b). The pure and doped films were found to be hexagonal wurtzite structure. The positions were indexed to (1 0 0), (0 0 2), (1 0 1), (1 0 2), (1 1 0), (1 0 3), (1 1 2) and (2 0 1) plane and peak positions were found to be in accordance with the JCPDS card no. 36-1451 of ZnO. From the XRD data it is evident that, there are no additional peaks due to Pb^{2+} ions substitution. This clearly indicates that, the substitution of Zn^{2+} ions by Pb^{2+} ions has not altered the inherent wurtzite structure of ZnO. At the same time, a slight shift in the peak position of doped ZnO thin films was observed in comparison with undoped ZnO thin films as shown in Fig. 1(b). We observe that the intensity of the diffraction peaks increases when Pb is doped into the host ZnO thin film. The tendency indicates that the improvement in crystalline quality with raising Pb doping concentration. The observed lattice parameters of pure and doped ZnO nanocrystalline films are given in Table 1.

The average crystallite size has been inferred from 2θ and the full width at half maximum (FWHM) of the (h k l) peaks using Debye–Scherrer relation,

$$d = \frac{K\, \lambda}{\beta\, \cos\theta}$$

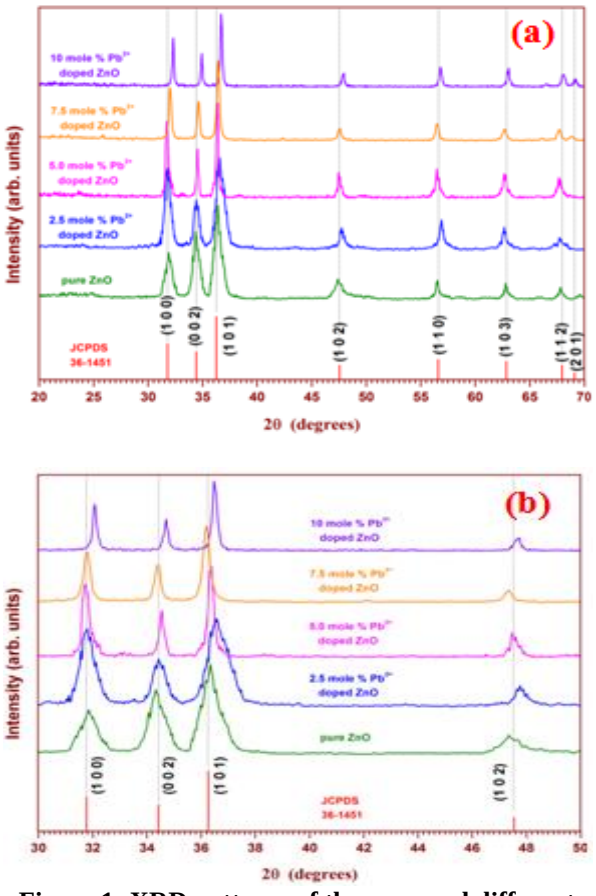

Figure 1: XRD patterns of the pure and different concentration of Pb^{2+} doped ZnO nanocrystalline thin films. [a] 2θ range between 20º and 70º and [b] 2θ range between 30º and 50º

where d is the average crystallite size (nm), K is the shape factor (0.9), λ is the wavelength of X-ray (1.5406 Å) Cu K_α radiation, θ is the Bragg angle, and β is the corrected line broadening of the nanoparticles. The average crystallite sizes of ZnO:Pb^{2+} (0, 2.5, 5.0, 7.5 and 10.0 mole %) are 9.28, 11.13, 19.72, 23.09 and 28.24 nm, respectively. Furthermore, it can be seen that the crystallite size of Pb doped ZnO increases with the increasing dopant concentration. From Fig. 1(b) we observed that the peak broadening is decreases with the increasing Pb^{2+} concentration. This is attributed to the larger ionic radius (1.33 Å) of Pb^{2+} ions that have replaced the Zn^{2+} ions with smaller ionic radius (0.88 Å) [46]. Hence the crystallite sizes of doped ZnO decreases with increasing concentration of Pb. This result was confirmed by SEM and it is shown in Fig. 2(a and b). It is also observed that the surface of the prepared nanocrystalline film is smooth and uniform with no cracks on it.

Table 1: The observed structural data from XRD measurements for pure and Pb^{2+}doped ZnO thin film. (*JCPDS file No. 36-1451)

Sample name	Dopant concentration (mole %)	Calculated parameters		
		a=b (Å)	c (Å)	Volume ($Å^3$)
pure ZnO	–	3.2414 *3.2498	5.1887 *5.2066	47.212 *47.621
Pb^{2+} doped ZnO	2.5	3.2859	5.2469	49.062
	5.0	3.3215	5.3147	50.778
	7.5	3.3063	5.5176	52.235
	10.0	3.3921	5.4473	54.281

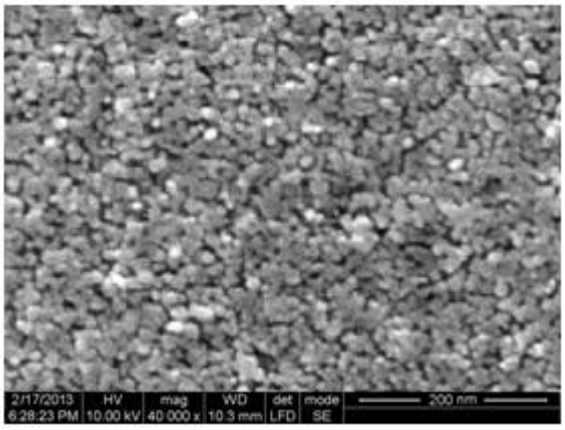

Figure 2(a): SEM image of pure ZnO

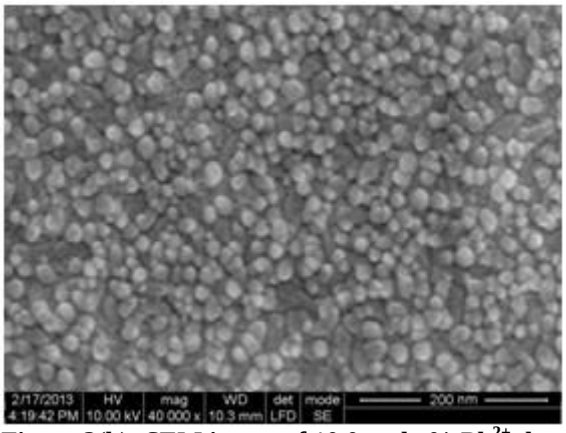

Figure 2(b): SEM image of 10.0 mole % Pb^{2+} doped ZnO

The variation of c/a ratio features with respect to concentration of dopant in ZnO lattices is shown in Fig. 3. The c/a ratio also confirms that the variation is much noticeable particularly for the concentration such as 7.5 and 10.0 mole %. More interestingly, when 'a' is seen enhanced 'c' seems to have dropped, which suggests that the non-uniform lattice expansion in the 'c' axis with respect to 'a' axis of the unit cell. It can also be attributed to the more directional incorporation of the substituting dopant atoms in one axis than the other axis. However when the host atoms (Zn) are substituted by Pb atoms the cell structure with different lattice parameter could occur, such behavior is clearly brought out here. The c/a ratio suggesting that Pb^{2+} plays a crucial role in the stacking of substituting atoms in the host lattice, probably through influencing the mobility of substituting atoms.

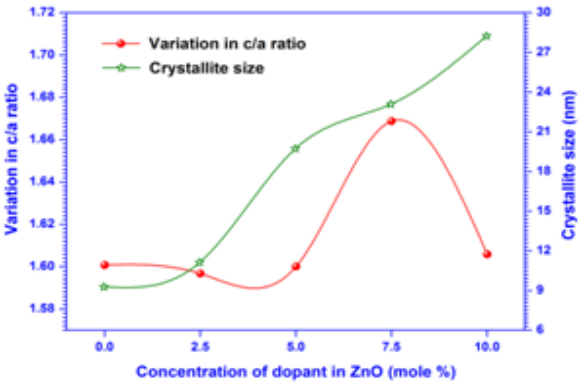

Figure 3: The variation c/a ratio and crystallite size with different dopant concentrations (mole %) of Pb^{2+} in ZnO

3.2. Electrical studies

The σ_{dc} of pure and doped (2.5, 5.0, 7.5 and 10.0 mole %) ZnO thin films are provided in Fig. 4. With increasing temperature, the dc conductivity of pure and doped ZnO thin films is found to increase. These results are consistent with the electronic

properties of semiconductor materials. At low temperatures, most of the free carriers in a semiconductor do not have sufficient energy to jump from one level to another level. When the temperature increases slowly, the carrier concentration increases in the conduction band, resulting in an increase in the σ_{dc} with increasing temperature [47]. The σ_{dc} value at room temperature has been found to increase by more than two orders of magnitude from pure ZnO film. It is well known that ZnO always exhibits high levels of unintentional n-type conductivity with an electron concentration of the order of 10^{18} cm^{-3}. Also it is well known that the electrical conductivity of ZnO samples at room temperature is due to intrinsic defects created by oxygen vacancies. These defects introduce donor states in the forbidden band slightly below the conduction band and hence resulting in the conducting behavior of ZnO increases [48]. This electrical conductivity is controlled by the intrinsic defects generated during synthesis and by the presence of dopants. From the observed result of increase in σ_{dc} of ZnO nonocrystalline film on Pb^{2+} doping, it seems that the Pb^{2+} doping affects the defect chemistry of the ZnO. Therefore, we may believe that the addition of dopants (considered in the present study) in ZnO increase the concentration of intrinsic donors. This intrinsic donor concentration increases with increase of dopant concentration up to 5.0 mole% doped ZnO films, which intern increases the electrical conductivity. As the dopant concentration further increases (more than 5.0 mole % of Pb^{2+}) in ZnO nanocrystalline film we observed significant degradation in σ_{dc}. This was because that some dopant atoms did not occupy the Zn site in crystal lattice of ZnO nanocrystalline film, but then assemble at the crystal grain boundary. As such, defects of the boundary acted as a scattering center and they become electrically inactive, hence they deteriorated the σ_{dc} [49]. It is important to note that the (σ_{dc}) of all the doped ZnO nanocrystalline films is higher than that of pure ZnO nanocrystalline film.

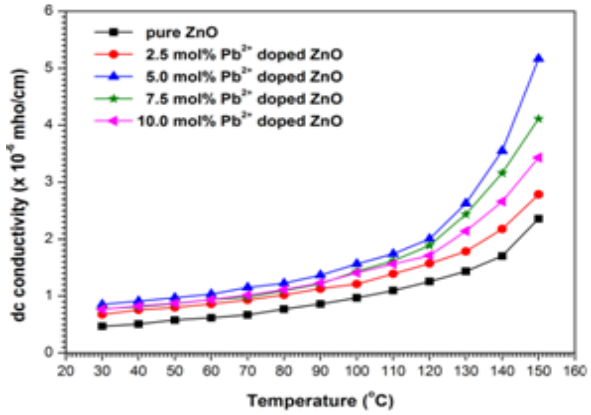

Figure 4: DC conductivities for pure and different concentration of Pb^{2+} doped ZnO nanocrystalline films

The dielectric constant (ε_r), dielectric loss factor (tanδ) and AC electrical conductivity (σ_{ac}) values obtained in the present study are shown in Fig. 5-7. The ε_r obtained (with frequency 1 kHz) for the pure ZnO film (5.642) is very small when compared to that observed for the bulk crystal (8.66) [50].

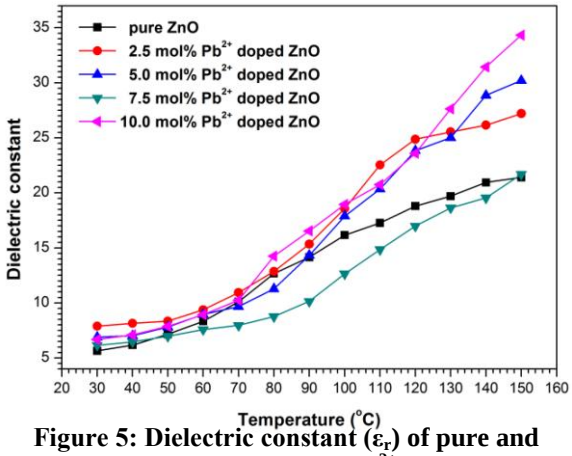

Figure 5: Dielectric constant (ε_r) of pure and different concentrations of Pb^{2+} doped ZnO nanocrystalline films at 1 kHz frequency

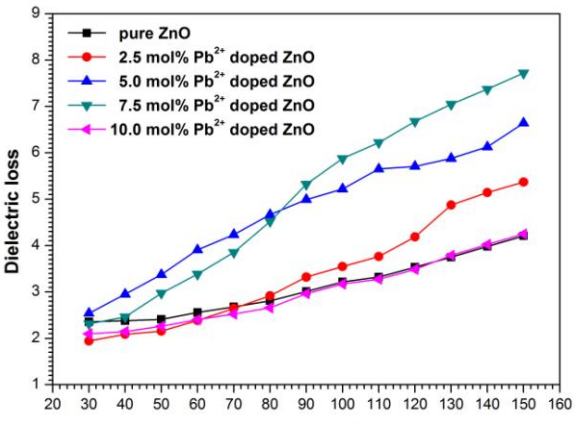

Figure 6: Dielectric loss (tan δ) of pure and different concentrations of Pb^{2+} doped ZnO nanocrystalline films at 1 kHz frequency

The electrical parameters, viz. ε_r, tanδ and σ_{ac} observed in the present study are increased with the increase in temperature for all the pure and doped nanocrystalline films considered in the present study indicating that the conductivity is thermally activated. The σ_{ac} of doped films is higher than that of pure ZnO film. The observed σ_{ac} values are found to be more than σ_{dc} values. The decreasing ac electrical conductivity at higher concentration (10 mole%) of doping level is explained by the feature that the excess of introduced doping atoms are segregated into the grain boundaries where they become electrically inactive. It can be explained considering that the presence of higher dopant Pb^{2+} ions (10 mole%) introduce defects such as zinc interstitials and oxygen

vacancies in the ZnO crystal lattice. These defects tend to segregate at the grain boundaries due to diffusion process and therefore facilitate the formation of grain boundary defect barrier leading to blockage to the flow of charge carriers. This in turn decreases the conductivity of the higher concentration doped ZnO nanocrystalline films.

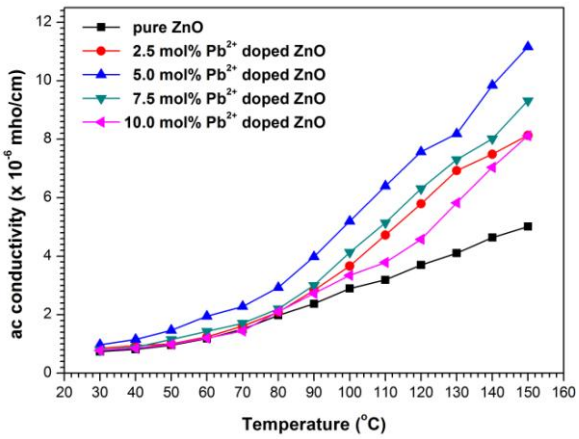

Figure 7: AC conductivity (σ_{ac}) of pure and different concentrations of Pb^{2+} doped ZnO nanocrystalline films at 1 kHz frequency

The variation of σ_{ac} with frequency for pure and doped ZnO films is shown in Fig. 8. From the Fig. 8 it is observed that the σ_{ac} gradually increases with the increase in frequency of applied ac field because the increase in frequency enhances the migration of electron [51] (Wang et al 2006) in the pure and doped ZnO films. It can be seen that the ac conductivity is increasing slowly at low frequency region, while it increases sharply at high frequency region. The increase in conductivity indicates that the rate of mobile ions increases. The rate of mobile ions are enhanced once the frequency of an applied field increases; resulting in an increase of conductivity.

The electrical resistivity of nanocrystalline material is higher than that of both conventional coarse grained polycrystalline material and alloys. The magnitude of electrical resistivity and hence the conductivity in composites can be changed by altering the size of the electrically conducting component. The σ_{dc} and σ_{ac} values observed in the present study are very small (i.e. the resistivities are very large). When the crystal (grain) size is smaller than the electron mean free path, grain boundary scattering dominates and hence electrical resistivity is increased.

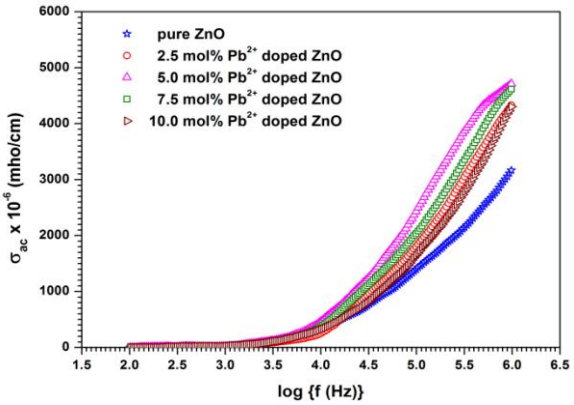

Figure 8: The Variation of ac conductivity with frequency for pure and different concentration of Pb^{2+} doped ZnO nanocrystalline film at room temperature.

IV. Conclusions

Pb doped ZnO nanocrystalline films were prepared on quarts glass plate by CBD technique. The XRD results indicate the Pb doping does not change the wurtzite structure of ZnO in all the doped samples. Within the XRD detection limit, no secondary phases are found. The dielectric loss and dielectric constant was found to decrease with the increase in temperature. AC and DC conductivities were found to increase with the increase in temperature which shows the temperature dependent electrical behavior of the samples. AC conductivity of the prepared samples was found to increase with increase in frequency. All these results indicate that the Pb doping concentration has great influences on the structural and electrical properties of ZnO nanocrystalline films.

References

[1] F. Paraguay, W. Estrada, D.R. Acosta, E. Andrade, M. Miki-Yoshida, Thin Solid Films, 350 (1999) 192 - 202.
[2] D. J. Goyal, C. Agashe, M. G. Takwale, B. R. Marathe, V. G. Bhide, J. Mater. Sci., 27 (1992) 4705.
[3] D. C. Look, Mater. Sci. Eng. B: Solid-State Mater. Adv. Technol., 80 (2001) 383.
[4] S. O. Kucheyev, J. S. Williams, C. Jagadish, J. Zou, C. Evans, A. J. Nelson, A. V. Hamza, Phys. Rev. B, 67(2003) 094115.
[5] A. Ashour, M. A. Kaid, N. Z. El-Sayed, A. A. Ibrahim, Appl. Surf. Sci., 252 (2006) 7844 - 7848.
[6] T. Mohammad, A. A. Hashim, M. H. Al-Maamory, Mater. Chem. and Phy., 99 (2006) 382 - 387.
[7] G. Hua, Y. Zhang, J. Zhang, X. Cao, W. Xu, L. Zhang, Materials Letters, 62 (2008) 4109 - 4111.

[8] D. A. Lamb, S.J.C. Irvine, Journal of Crystal Growth, 273 (2004) 111.
[9] Z. W. Pan, Z. R. Dai, Z. L. Wang, Science, 291 (2001) 1947.
[10] B. Y. Oh, M. C. Jeong, T. H. Moon, W. Lee, J. M. Myoung, J. Y. Hwang, D. S. Seo, J. Appl. Phys., 99 (2006) 124505.
[11] H. T. Wang, B. S. Kang, F. Ren, L. C. Tien, P. W. Sadik, D. P. Norton, S. J. Pearton, Jenshan Lin, Appl. Phy. Lett., 86 (2005) 243503.
[12] L. C. Tien, P. W. Sadik, D. P. Norton, L. F. Voss, S. J. Pearton, H. T. Wang, B. S. Kang, F. Ren, J. Jun, J. Lin,Appl. Phy. Lett., 87 (2005) 222106.
[13] V.R. Shinde, T.P. Gujar, C.D. Lokhande, Sens. Actuators B, 120 (2007) 551 - 559.
[14] Y. C. Kong, D. P. Yu, B. Zhang, S. Q. Feng, Appl. Phys. Lett., 78 (2001) 407.
[15] K. Nomura, H. Ohta, K. Ueda, T. Kamiya, M. Hirano, H. Hosono, Science, 300 (2003) 1269 - 1272.
[16] Y. B. Li, Y. Bando, D. Golberg, Appl. Phys. Lett., 84 (2004) 3603.
[17] J. H. Lee, Y. W. Chung, M. H. Hon, I. C. Leu, Appl. Phys. A, 97/2 (2009) 403 - 408.
[18] Y. W. Heo, L. C. Tien, Y. Kwon, D. P. Norton, S. J. Pearton, B. S. Kang, F. Ren, Appl. Phys. Lett., 85 (2004) 2274.
[19] A. Bakin, A. El-Shaer, A. C. Mofor, M. Al-Suleiman, E. Schlenker, A. Waag, Physica Stat. Solidi – C, 4/1 (2007) 158 - 161.
[20] E. Fortunato, P. Barquinha, A. Pimentel, L. Pereira, A. Gonçalves, A. Marques, R. Martins, Appl. Phys. Lett., 85 (2004) 2541.
[21] T. Prasada Rao. M.C. Santhoshkumar, App. Surf. Sci., 255 (2009) 4579 - 4584.
[22] B. J. Lokhande, M. D. Uplane, Appl. Surf. Sci., 167 (2000) 243.
[23] B. J. Lokhande, P. S. Patil, M. D. Uplane, Mater. Lett., 57 (2002) 573 - 579.
[24] F. Paraguay D., J. Morales, W. Estrada L., E. Andrade, M. Miki-Yoshida, Thin Solid Films, 366 (2000) 16 - 27.
[25] P. Nunes, E. Fortunato, R. Martins, Thin Solid Films, 383 (2001) 277 - 280.
[26] A. Mosbah, M.S. Aida, J. Alloys Comp. 515 (2012) 149–153.
[27] J.J. Ding, H.X. Chen, X.G. Zhao, S.Y. Ma, J. Phys. Chem. Solids 71 (2010) 346–350.
[28] R. Vinodkumar, I. Navas, S.R. Chalana, K.G. Gopchandran, V. Ganeshan, Reji Philip, V.P. Mahadevan Pillai, Appl. Surf. Sci. 257 (2010) 708–7016.
[29] W.I. Park, S.J. An, J.L. Yang, G.C. Yi, S. Hong, T. Joo, M. Kim, J. Phys. Chem. B 108 (2004) 15457–15460.
[30] Z.Q. Ma, W.G. Zhao, Y. Wang, Thin Solid Films 515 (2007) 8611–8614.
[31] J. Zhong, S. Muthukumar, Y. Chen, Y. Lu, Appl. Phys. Lett. 83 (2003) 3401–3403.
[32] Takahiro Yamada, Aki Miyake, Seiichi Kishimoto, Hisao Makino, Naoki Yamamoto, Tetsuya Yamamoto, Surf. Coat. Technol. 202 (2007) 973–976.
[33] C. Xu, M. Kim, J. Chun, D. Kim, Appl. Phys. Lett. 86 (2005) 1331071–1331073.
[34] V. Bhosle, A. Tiwari, J. Narayan, Appl. Phys. Lett. 88 (2006) 0321061–0321063.
[35] S.Y. Bae, H.W. Seo, J. Park, J. Phys. Chem. B 108 (2004) 5206–5210.
[36] Dongyan Zhang, Hiromi Yabe, Eri Akita, Pangpang Wang, Ri-ichi Murakami, J. Appl. Phys. 109 (2011) 1043181–1043185.
[37] Haixia Chen, Jijun Ding, Feng Shi, Yingfeng Li, Wenge Guo, J. Alloys Comp. 534 (2012) 59–63.
[38] S. Eustis, D.C. Meier, M.R. Beversluis, B. Nikoobakht, ACS Nano 2 (2008) 368–374.
[39] S.-M. Zhou, X.-H. Zhang, X.-M. Meng, S.-K. Wu and S.-T. Lee, Phys. Status Solidi A, 202 (2005) 405–410.
[40] P Nunes, E Fortunato, P Tonello, F Braz Fernandes, P Vilarinho, R Martins, Vacuum, 64 (2002) 281–285
[41] Dewei Chu, Yu-Ping Zeng, Dongliang Jiang, Materials Letters, 60 (2006) 2783–2785
[42] N. Nithya, S. Rugmini Radhakrishnan, International Journal of Physical, Chemical & Mathematical Sciences, 2 (2013) 45-54.
[43] N. Nithya, S. Rugmini Radhakrishnan, International Journal of Engineering Research and Technology 2 (2013), 1649-1655.
[44] B. D. Cullity (Ed.), Elements of X-ray diffraction, Addison-Wesly, New York, 1997, p.102.
[45] R.S.S. Saravanana, D. Pukazhselvan, C.K. Mahadevan, Journal of Alloys and Compounds, 517 (2012) 139-148
[46] http://en.wikipedia.org/wiki/Ionic_radius
[47] J. F. Condeles, T. Ghilardi Netto, M. Mulato, Nucl. Instrumand Meth. A 577 (2007) 724–728.
[48] T. K. Gupta, J. Mater. Res. 7 (1992) 3280-3295.
[49] E. Chikoidze, Y. Dumont, F. Jomard, O. Gorochov, Thin Solid Films 515 (2007) 8519-8523
[50] Y. Yang, W. Guo, X. Wang, Z. Wang, J. Qi, Y. Zhang, Nano Lett. 12 (2012) 1919-1922
[51] X.B. Wang, C. Song, K.W. Geng, F. Zeng, F. Pan, Journal of Physics D: Applied Physics 39 (2006) 4992 - 4998.